RSC Advances




ROYAL SOCIETY OF CHEMISTRY

www.rsc.org/advances

# Simultaneous influence of $Zn^{2+}$/ $Mg^{2+}$ on luminescent behaviour of $La_2O_3$: $Tm^{3+}$-$Yb^{3+}$ phosphor

Astha Kumari, Anurag Pandey, Riya Dey and Vineet Kumar Rai*

Laser and Spectroscopy Laboratory, Department of Applied Physics

Indian School of Mines, Dhanbad-826004, Jharkhand, India



*** Author's to whom Correspondence be made:**

Email address: vineetkrrai@yahoo.co.in; rai.vk.ap@ismdhanbad.ac.in

Phone no.:+91-326-223 5404

## Abstract

The structural characterizations of $La_2O_3$ phosphors doped/codoped with $Tm^{3+}$, $Yb^{3+}$ ions synthesized by urea assisted solution combustion technique have been performed by using X-ray diffraction analysis, Fourier Transform Infrared spectroscopy and Scanning electron microscopy. The codoping with $Zn^{2+}$/$Mg^{2+}$ ions causes an increase in the particle size and aggregation of the $La_2O_3$: $Tm^{3+}$- $Yb^{3+}$ phosphor. The upconversion (UC) study under 980 nm excitation shows four UC emission bands centred around 476 nm ($^1G_4 \rightarrow {}^3H_6$), 653 nm ($^1G_4 \rightarrow {}^3F_4$), 702 nm ($^3F_2 \rightarrow {}^3H_6$) and 795 nm ($^1G_4 \rightarrow {}^3H_5$). The effect of codoping with $Zn^{2+}$ and $Mg^{2+}$ ions in the $Tm^{3+}$-$Yb^{3+}$ codoped $La_2O_3$ phosphor has been investigated. The decay curve analysis of the prepared phosphors to understand the mechanism involved in the upconversion emission intensity variation due to codoping with $Zn^{2+}$/ $Mg^{2+}$ ions has been made. The purity of colour emitted from the sample does not show any change with varying the pump power density.


***Keywords:*** Phosphors, Rare earths, Codoping effect, Energy transfer, Colour coordinates.

## 1. Introduction

The luminescent materials due to its excellent luminescent behaviour have found its wide applications in the field of optical data storage, lasers, temperature sensors, detection of infrared radiation, colour displays, biomedical diagnostics, upconverters, optical amplifiers, telecommunication, plasma display panels, high definition televisions ( HDTVs), light emitting diodes, cathode ray tubes (CRTs), finger print detection, scintillators, etc.[1-8]. In these materials, luminescence takes place due to energy transition within the energy levels of rare earth ions[1]. Rare earth ions (REs) are characterized by a partially filled 4f shell that is shielded by completely filled outer $5s^2$ and $5p^6$ orbital which causes sharp luminescence followed by the intra 4f shell transitions. The energy levels of the rare earth ions are therefore largely insensitive to the host environment in which they are placed and leads to their radiative transitions in solid hosts resemble to those of the free ions[9]. The lanthanide elements when incorporated in crystalline or amorphous hosts, exist in triply ionized state, or occasionally doubly ionized oxidation state.

The upconversion emission from the singly thulium doped luminescent materials has been observed by many researchers[10-14] but better luminescence was observed when thulium was codoped with ytterbium[12, 15-16]. This is possible because of the high absorption cross-section and favourable energy level structure of $Yb^{3+}$ ions for getting excited to the higher energy level upon 980 nm excitation[17, 18]. The selection of appropriate host material is still an essential task for the preparation of micro/nanocrystalline luminescent materials with efficient optical properties. Among various solid host materials, oxides and fluorides are mostly preferred because of their low cut-off phonon frequencies which results in less energy loss due to the non-radiative relaxation channels[19]. The $La_2O_3$, a solid material is expected to be suitable for preparation of highly luminescent phosphor material due to low cost, good

chemical durability and thermal stability, low phonon frequency (~400cm$^{-1}$) etc.[20, 21]. The lanthanum oxide has been considered as an attractive host material for codoping of triply ionised lanthanides owing to its comparable ionic radii. It is known that the codoping with rare-earth ions increases the pump efficiency and hence the intensity of the upconversion (UC) emission, but the effect of codoping with non-rare-earth ions has been studied rarely. Researchers have studied the effect of co-doping with Zinc and magnesium individually on its electrical, structural, electrochemical and of course the photoluminescence properties of rare earth doped/codoped luminescent materials. The UC luminescence enhancement of about ~ 37 times for the green band at ~ 551 nm in the $Nd^{3+}$-$Yb^{3+}$-$Zn^{2+}$ codoped $Y_2O_3$ phosphor upon excitation at 980 nm has been observed by Dey et al.[22]. The effect of magnesium doping on the structural as well as optical properties of $Zn_2GeO_4$: Mn phosphor has been reported by Anoop et al.[23]. The enhancement of about ~ 60 times in the green UC intensity has been observed due to the codoping with $Mg^{2+}$ ions in $Er^{3+}$-$Yb^{3+}$ codoped $CaAl_{12}O_{19}$ phosphor[24]. But the effect of codoping of a combination of non-rare earth ion like Zinc and Magnesium simultaneously on the UC luminescence study have not been reported till now to the best of our knowledge.

Here, we report the synthesis and characterization of the prepared phosphors. The near infrared (NIR) to visible frequency UC emission in the $Tm^{3+}$-$Yb^{3+}$co-doped $La_2O_3$ phosphor and the effect of $Zn^{2+}$-$Mg^{2+}$ codoping on the UC emission arising from the thulium ions has been studied. The XRD, FTIR, pump power dependence and decay curve analysis has been explored to get the information about the mechanism involved in the frequency UC emissions. The effect of the variation of pump power density on the colour emitted from the developed phosphor has also been confirmed.

## 2. Experimental

### *2.1 Material synthesis*

The $Tm^{3+}$, $Tm^{3+}$-$Yb^{3+}$, $Tm^{3+}$-$Yb^{3+}$-$Zn^{2+}$ and $Tm^{3+}$- $Yb^{3+}$- $Zn^{2+}$-$Mg^{2+}$ doped/codoped $La_2O_3$ phosphors have been prepared by combustion route. The compositions taken for the synthesis of these phosphor powders are as follows

$$(100\text{-}p\text{-}q)\ La_2O_3 + p\ Tm_2O_3 + q\ Yb_2O_3 \quad \text{..... (1)}$$

where $p$ = 0.1 mol% and $q$ = 0.0, 1.0, 3.0, 5.0 mol% and

$$(100\text{-}p\text{-}q\text{-}r)\ La_2O_3 + p\ Tm_2O_3 + q\ Yb_2O_3 + r\ ZnO \quad \text{..... (2)}$$

where $p$ = 0.1 mol% and $q$ = 3.0 mol % and $r$ = 5.0, 10.0, 15.0 and 25.0 mol % and

$$(100\text{-}p\text{-}q\text{-}r\text{-}s)\ La_2O_3 + p\ Tm_2O_3 + q\ Yb_2O_3 + r\ ZnO + s\ MgCO_3 \quad \text{..... (3)}$$

where p= 0.1 mol% and q= 3.0 mol %, r = 15.0 mol % and s = 3.0, 5.0, 7.0 and 10.0 mol%. Stoichiometric amounts of the precursor chemicals were taken and treated with nitric acid to form their nitrates. After that they were mixed together and then appropriate amount of urea solution was mixed with the nitrate mixtures. The obtained solutions were stirred at 950 rpm for about 3 hours at a constant temperature of 60 $^0$C to get gel like products. The gels were then transferred into different alumina crucibles and kept inside an electric furnace at 550 $^0$C. Within 2-5 minutes combustion process completed. The obtained whitish products were grinded into fine powder form and further annealed at 800 $^0$C for 3 hours. The annealed samples were used for the structural and optical analysis.

### *2.2 Characterization*

For the structural study, the X-ray diffraction (XRD) analysis and Scanning electron microscopy (SEM) have been done using Bruker D8 advanced X-ray diffractometer and HITACHI (S-3400N) Scanning Electron Microscope respectively. To study the presence of impurity contents in the samples, the Fourier Transform Infrared (FTIR) spectra of the samples were recorded in the 400-4000 $cm^{-1}$ spectral region on Perkin Elmer Spectrum RX1 spectrophotometer. The UC emission spectra of the phosphor powders were recorded through a monochromator attached with a photomultiplier tube (PMT) upon excitation with 980 nm continuous wave (CW) diode laser. The lifetime analysis were performed by chopping the 980 nm laser beam by using a mechanical chopper and measurements were recorded with the help of quick start digital oscilloscope. All the measurements were performed at room temperature.

## 3. Results and discussion

### *3.1 XRD Analysis*

The powder XRD patterns of the $Tm^{3+}$-$Yb^{3+}$; $Tm^{3+}$-$Yb^{3+}$-$Zn^{2+}$ and $Tm^{3+}$- $Yb^{3+}$- $Zn^{2+}$-$Mg^{2+}$ codoped $La_2O_3$ phosphor samples were done between the range of 20 - 90 degree (Fig. 1). All the XRD patterns have the same base line and same pattern which shows that the crystal structure as well as the phase of these prepared materials have not been altered due to codoping with rare-earth as well as non rare-earth elements. A large number of intense diffraction peaks for different 2θ values at ~ 26.71, ~ 29.6, ~ 30.55, ~ 39.94, ~ 46.66, ~ 52.72, ~ 55.53, ~ 63.04, ~ 72.88, ~ 75.94, ~ 79.42, ~ 81.37, ~ 84.37, ~ 85.72 corresponding to the diffraction from the (100), (002), (011), (012), (110), (103), (112), (202), (203),(211), (114) , (122), ( 015), (300) planes respectively have been observed. The observed structure of the prepared phosphors were indexed suitably with JCPDS file no.74-

1144 that shows the hexagonal phase of the $La_2O_3$ with lattice parameters a=b=3.93 A° and c= 6.12 A°.

The average crystallite size of synthesized phosphors has been calculated using Debye–Scherrer equation[20]

$$d = 0.89\lambda / \beta \cos\theta \quad \text{..... (4)}$$

where "d" is the crystallite size, "λ" is the wavelength of X-ray (~ 1.5405 $A^0$) used , "β" is the full-width half maxima (FWHM) and "θ" is the diffraction angle. The calculated values of the average crystallite size are found to be ~13 nm, ~15 nm and ~25 nm for $La_2O_3$: $Tm^{3+}$-$Yb^{3+}$, $La_2O_3$: $Tm^{3+}$- $Yb^{3+}$- $Zn^{2+}$ and $La_2O_3$: $Tm^{3+}$- $Yb^{3+}$- $Zn^{2+}$ -$Mg^{2+}$ phosphors respectively.

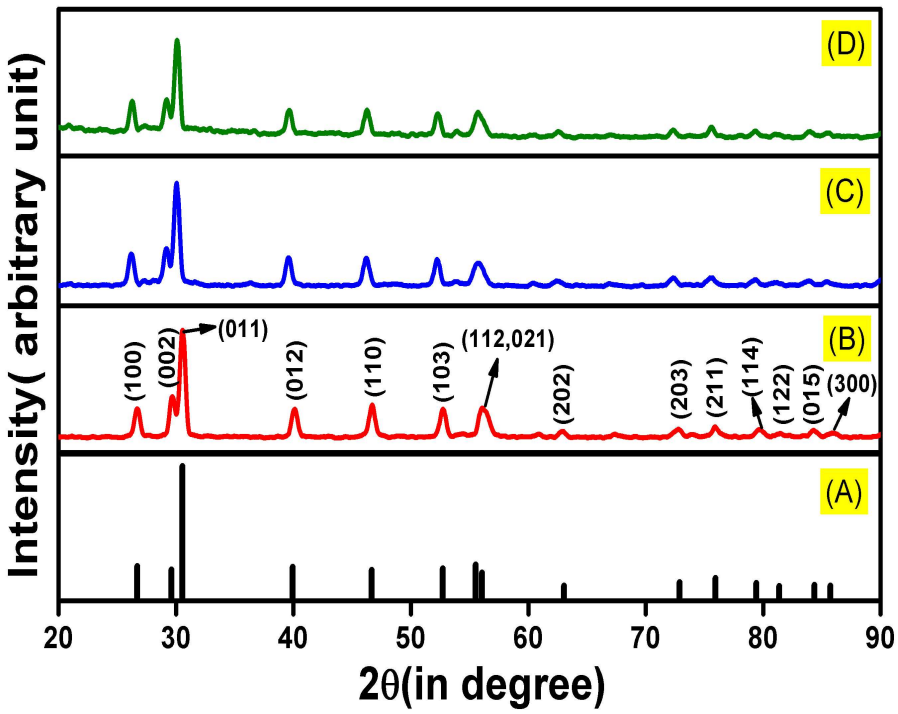


**Fig. 1:** XRD pattern of (A) JCPDS file no.74-1144 (B) $Tm^{3+}$-$Yb^{3+}$(C) $Tm^{3+}$-$Yb^{3+}$-$Zn^{2+}$ and (D) $Tm^{3+}$-$Yb^{3+}$-$Zn^{2+}$-$Mg^{2+}$ codoped $La_2O_3$ phosphors.

In addition to Debye-Scherrer method the crystallite size of the prepared materials have also been estimated with the help of Williamson-Hall Analysis which satisfies the equation[25].

$$\beta \cos\theta = ( 0.89 \lambda / d ) + 4 \varepsilon \sin \theta \quad \text{..... (5)}$$

where "ε" is the strain present in the sample and other symbols have their usual meanings. The strain present in the material and the crystallite size could be extracted from the slope and the intercept of the 4sinθ versus βcosθ plot respectively. The Williamson-Hall plots for $Tm^{3+}$- $Yb^{3+}$, $Tm^{3+}$- $Yb^{3+}$- $Zn^{2+}$ and $Tm^{3+}$- $Yb^{3+}$- $Zn^{2+}$ -$Mg^{2+}$ codoped $La_2O_3$ phosphors are shown in Fig.2.

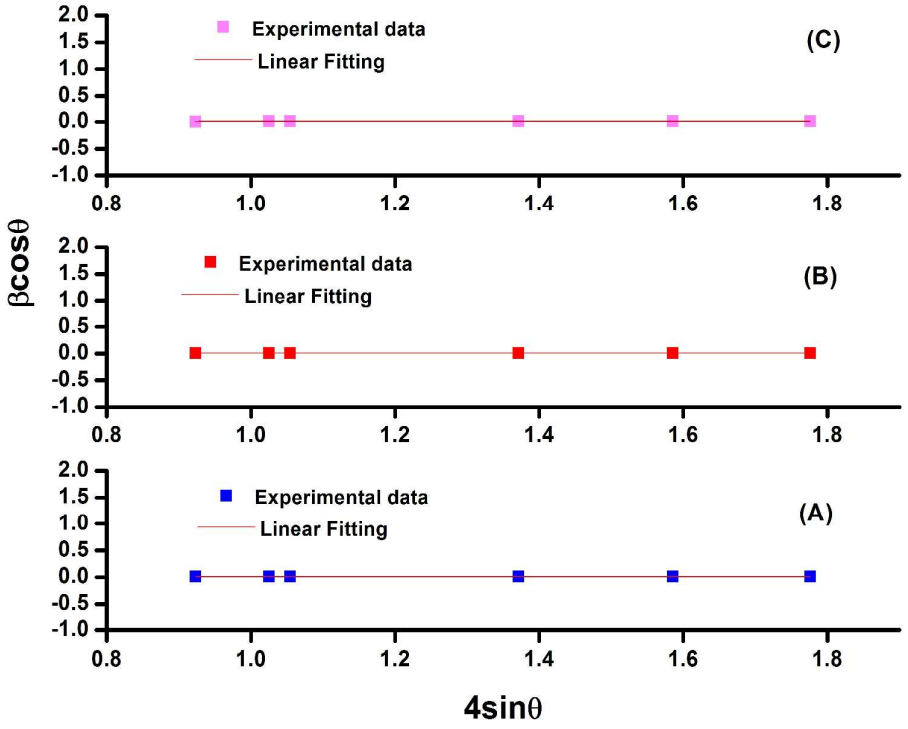


**Fig. 2:** Williamson-Hall plot for (A) $Tm^{3+}$-$Yb^{3+}$ (B) $Tm^{3+}$-$Yb^{3+}$-$Zn^{2+}$ and (C) $Tm^{3+}$-$Yb^{3+}$-$Zn^{2+}$-$Mg^{2+}$ codoped $La_2O_3$ phosphors.

The calculated values of the crystallite sizes as calculated by Williamson-Hall analysis are 15.65 nm, 16.81 nm and 28.29 nm for $La_2O_3$: $Tm^{3+}$- $Yb^{3+}$, $La_2O_3$: $Tm^{3+}$- $Yb^{3+}$- $Zn^{2+}$ and $La_2O_3$: $Tm^{3+}$- $Yb^{3+}$- $Zn^{2+}$ -$Mg^{2+}$ phosphors respectively. Also, by analysing the results it can be concluded that the crystallite size calculated by both the methods (Debye-Scherrer Method and Williamson-Hall method) for all the three samples are comparable and a slight increase

in the crystallite size is observed as we move from $La_2O_3$: $Tm^{3+}$- $Yb^{3+}$ to $La_2O_3$: $Tm^{3+}$- $Yb^{3+}$- $Zn^{2+}$ -$Mg^{2+}$ via $La_2O_3$: $Tm^{3+}$- $Yb^{3+}$- $Zn^{2+}$ phosphors. The crystallite size in each case was found to be in the nanometer range which indicates that the developed phosphors are nanocrystalline in nature.

***3.2 FTIR Spectroscopy***

The FTIR of the prepared materials annealed at 800 $^0$C temperature have been recorded in the 400-4000 $cm^{-1}$ region (Fig.3). The presence of different impurity contents in the prepared materials have been traced by matching the vibrational frequencies corresponding to each impurity contents in the FTIR spectrum. From the FTIR spectrum of the prepared samples it can be concluded that the functional groups like -OH, -CH and -NO are present in all the samples. The peaks observed around ~ 3613 $cm^{-1}$ and ~ 2382 $cm^{-1}$ are due to asymmetric stretching vibration of O-H. The peak around ~ 2930 $cm^{-1}$ and ~ 1475 $cm^{-1}$ are due to C-H and N-O stretching vibrations respectively. It is also observed from the FTIR spectrum that the presence of O-H impurity observed around ~ 3613 $cm^{-1}$ has been reduced in the case of $La_2O_3$: $Tm^{3+}$- $Yb^{3+}$- $Zn^{2+}$ -$Mg^{2+}$ phosphor compared to other cases. The peak around 650 $cm^{-1}$ is due to the lattice vibration of La-O.

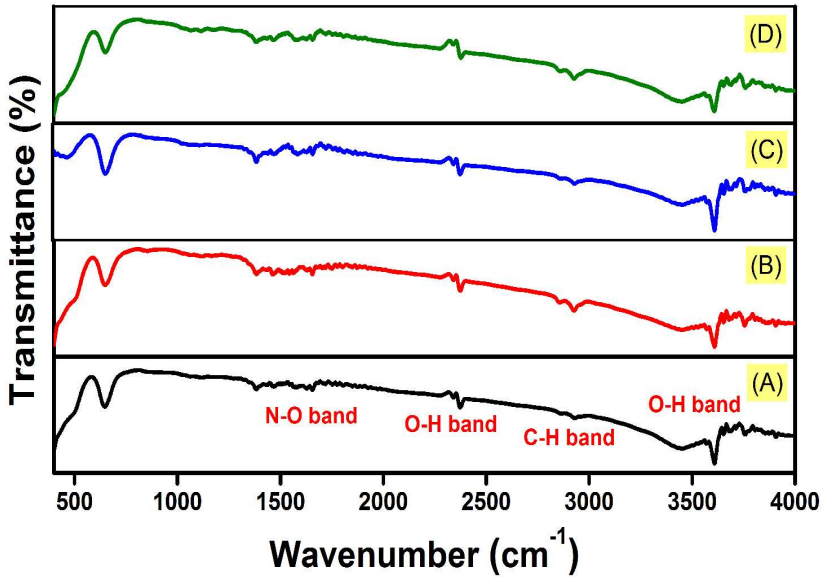


**Fig. 3:** FTIR spectrum of (A) $Tm^{3+}$ (B) $Tm^{3+}$-$Yb^{3+}$(C) $Tm^{3+}$-$Yb^{3+}$-$Zn^{2+}$ and (D) $Tm^{3+}$-$Yb^{3+}$-$Zn^{2+}$-$Mg^{2+}$ codoped $La_2O_3$ phosphors.

### *3.3 SEM Image*

The surface morphology and the crystallinity of solid host materials are important parameters which determine the emission characteristics. The microstructure analysis of $La_2O_3$: $Tm^{3+}$-$Yb^{3+}$ and $La_2O_3$: $Tm^{3+}$- $Yb^{3+}$- $Zn^{2+}$ -$Mg^{2+}$ samples has been performed with the help of SEM study (Fig. 4). From Fig. 4 it is clear that with $Zn^{2+}$/$Mg^{2+}$ ions codoping, the aggregation and particle sizes of the $La_2O_3$: $Tm^{3+}$- $Yb^{3+}$ phosphors increase. The SEM image shows that the particles are not uniformly distributed throughout the surface which is mainly caused by the inhomogeneous distribution of temperature during the synthesis of the material by the combustion technique. Also, it is clearly visualized that the particles are in the agglomerated form with its size in the micrometer range.

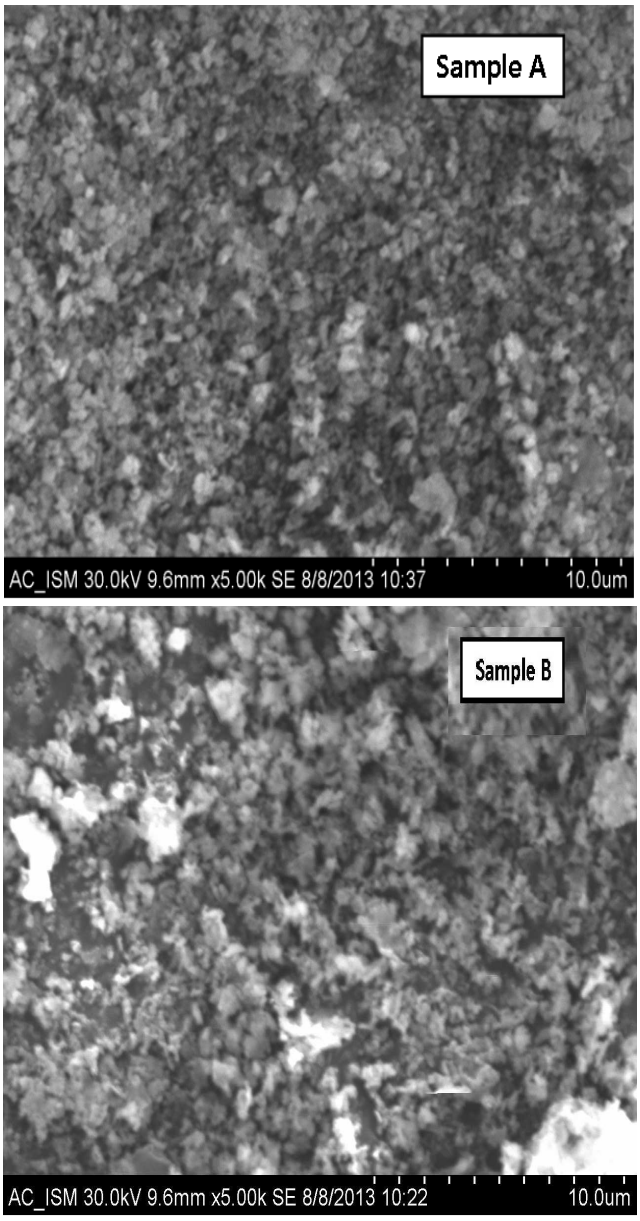


**Fig. 4:** SEM image of (a) $Tm^{3+}$-$Yb^{3+}$ codoped $La_2O_3$ phosphor (b) $Tm^{3+}$-$Yb^{3+}$-$Zn^{2+}$-$Mg^{2+}$ codoped $La_2O_3$ phosphor.

### *3.4 Upconversion emissions study of $La_2O_3$: $Tm^{3+}$- $Yb^{3+}$ phosphor*

The room temperature frequency upconversion spectra of the $Tm^{3+}$/$Tm^{3+}$-$Yb^{3+}$ doped/codoped $La_2O_3$ phosphor powders upon excitation with 980 nm CW diode laser have been recorded within 450–900 nm wavelength range (Fig. 5). From Fig. 5, it is clear that no UC emission has been observed under a 980 nm diode laser excitation from singly $Tm^{3+}$

doped $La_2O_3$ phosphor. But in case of $La_2O_3$: $Tm^{3+}$-$Yb^{3+}$ phosphor four UC emission bands have been observed around 476 nm, 653 nm , 702 nm and 795 nm corresponding to the $^1G_4 \rightarrow {}^3H_6$, $^1G_4 \rightarrow {}^3F_4$, $^3F_2 \rightarrow {}^3H_6$ and $^1G_4 \rightarrow {}^3H_5$ transitions respectively.

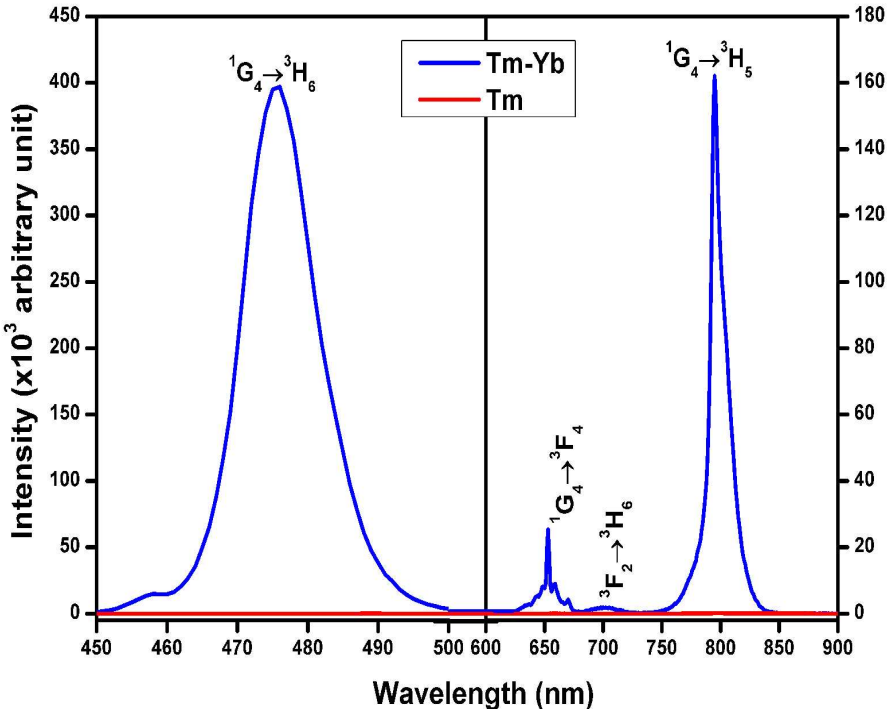


**Fig. 5:** The upconversion emission spectrum for $Tm^{3+}$ / $Tm^{3+}$-$Yb^{3+}$ codoped $La_2O_3$ phosphors.

To get the optimum UC intensity the concentration of $Yb^{3+}$ ions is varied from 1.0 to 5.0 mol% by assuming the $Tm^{3+}$ ions concentration fixed at 0.1 mol%. The maximum UC emission intensity has been observed for the 0.1 mol% $Tm^{3+}$ + 3.0 mol% $Yb^{3+}$ combination. The light emitted from the phosphor appears blue in colour which could be detectable with the naked eyes. The required NIR photons for the origin of these UC bands can be explained with the help of the pump power dependence study.

It is well known that for extremely small upconversion rates the number of photons involved in populating the upconversion emitting level can be calculated directly from the slope value of the logarithmic plot of intensity versus pump power. But, as we increase the pump power

to a higher value the upconversion luminescence caused by 'n' photon absorption is found to obey the relation $I_{UC} < P^{n}$ [26].

We know that UC emission intensity ($I_{UC}$) is directly proportional to pump excitation power (P) in the low pump power region by the relation[27],

$$I_{UC} \propto P^{k} \qquad \text{..... (6)}$$

where "k" represents the number of pump photons required to excite the emitting states.

The slope values corresponding to 476 nm, 653 nm bands comes out to be ~ 1.93, ~ 2.08 which shows that both the blue and red emissions are due to two photon absorption process.

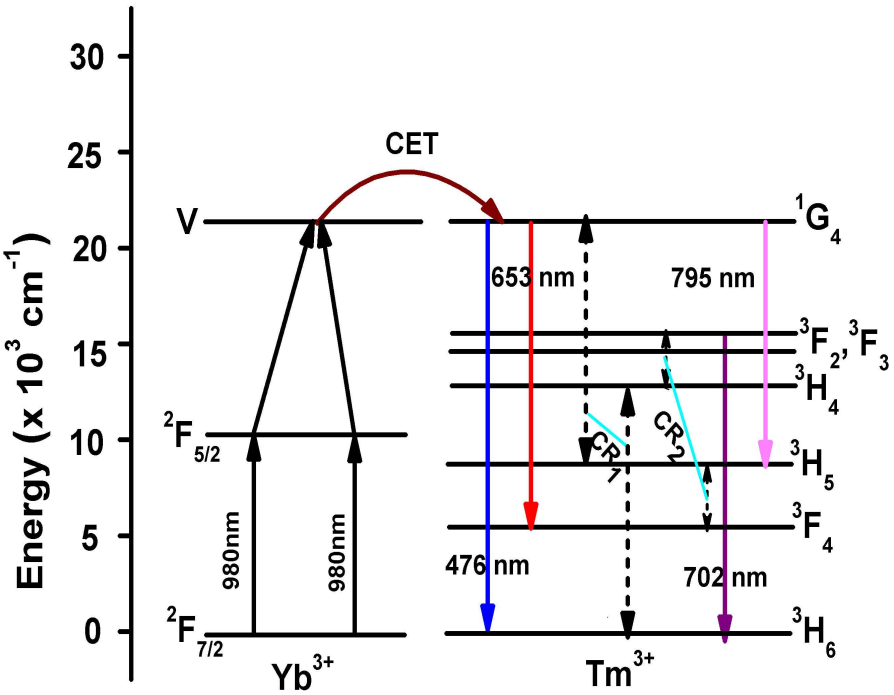


**Fig. 6**: Energy level diagram and energy transfer mechanism in $Tm^{3+}$-$Yb^{3+}$ codoped $La_2O_3$ phosphors.

The origin of the UC emission bands can be explained with the help of energy level diagram as shown in Fig. 6. The UC emissions which are observed from $Tm^{3+}$- $Yb^{3+}$ codoped $La_2O_3$ phosphor is due to the cooperative energy transfer (CET) from $Yb^{3+}$ to $Tm^{3+}$ ions only, as no UC emission is observed in singly doped $Tm^{3+}$:$La_2O_3$ phosphor. The $Yb^{3+}$ ions present in the $^2F_{7/2}$ ground state after absorption of 980 nm NIR photon get excited to the $^2F_{5/2}$ manifold. In the $^2F_{5/2}$ excited state, the excited donor ion transfers its excitation energy to the acceptor $Yb^{3+}$ ion in the $^2F_{5/2}$ state and the acceptor ion by absorbing this energy from donor further gets excited to the virtual level (V). The energy of the virtual level 'V' of $Yb^{3+}$ ion is in resonance with the $^1G_4$ (~21015 $cm^{-1}$) level of $Tm^{3+}$ ion. So, the $Yb^{3+}$ ions in the virtual level transfer its excitation energy to the $Tm^{3+}$ ions in ground state and the ground state $Tm^{3+}$ ions after absorbing this energy get excited to the $^1G_4$ level. Finally, the $Tm^{3+}$ ions in $^1G_4$ level transit downward to the $^3H_6$, $^3F_4$ (~5765 $cm^{-1}$) and $^3H_5$ (~8258 $cm^{-1}$) levels emitting blue, red and NIR emissions around 476 nm, 653 nm and 795 nm respectively. The $^3H_4$ (~12556 $cm^{-1}$) and $^3F_2$ (~15240 $cm^{-1}$) levels of $Tm^{3+}$ ion is populated by the cross-relaxation energy transfer mechanisms, $CR_1$ and $CR_2$ viz. ($^1G_4$, $^3H_6 \rightarrow$ $^3H_5$, $^3H_4$ ) and ($^3H_5$, $^3H_4 \rightarrow$ $^3F_4$, $^3F_2$ ) respectively. After that the $Tm^{3+}$ ions in the $^3F_2$ level decay radiatively to the $^3H_6$ level giving photon at ~ 702 nm corresponding to the $^3F_2 \rightarrow ^3H_6$ transition. The $^3F_3$ (~14627 $cm^{-1}$) level is populated by the non-radiative relaxation from the $^3F_2$ level followed by the emission of a phonon. The intensity ratio for the blue to red and blue to NIR emission peak intensity is found to be ~30 and ~ 5 respectively. This large UC emission intensity corresponding to the $^1G_4 \rightarrow {}^3H_6$ transition compared to the other transition is basically due to the direct cooperative energy transfer (CET) from the $Yb^{3+}$ ions to the $Tm^{3+}$ ions followed by the two NIR photons absorption.

### *3.5 Effect of $Zn^{2+}$ and $Mg^{2+}$ codoping in $La_2O_3$: $Tm^{3+}$- $Yb^{3+}$ phosphor*

From Fig. 7 it is clearly observed that the UC intensity of all the bands is enhanced with the addition of $Zn^{2+}$ and $Mg^{2+}$ ions in the $La_2O_3$: $Tm^{3+}$- $Yb^{3+}$ phosphor. The variation in UC intensity with different doping concentrations of $Zn^{2+}$ and $Mg^{2+}$ ions has been investigated. The enhancement about ~ 2 times for the blue UC bands has been observed with the codoping of 15.0 mol% $Zn^{2+}$ ions in the $Tm^{3+}$-$Yb^{3+}$ codoped $La_2O_3$ phosphor. It is also observed that the intensities of UC bands are further increased when the $Mg^{2+}$ ion is incorporated in the $Tm^{3+}$- $Yb^{3+}$-$Zn^{2+}$ codoped $La_2O_3$ phosphor. The optimum concentration of $Mg^{2+}$ ion is found to be 5.0 mol%. The enhancement of about ~ 36 times, ~ 34 times and ~ 11 times in the intensity of UC peaks at ~ 476 nm, ~ 653 nm and ~ 795 nm have been observed with the codoping of 5.0 mol% $Mg^{2+}$ ions compared to that of $Tm^{3+}$- $Yb^{3+}$ codoped $La_2O_3$ phosphor. The intensity of upconversion emission bands lying in the blue, red and NIR region is increased with increasing the $Zn^{2+}$ and $Mg^{2+}$ ions concentration upto 15.0 mol% and 5.0 mol% respectively. The enhancement in the UC intensity is because of the creation of the oxygen vacancies due to codoping with the $Zn^{2+}$/$Mg^{2+}$ ions in $La_2O_3$ phosphor. These oxygen vacancies act as sensitizers for energy transfer due to the mixing of charge transfer states[28]. This enhancement in the UC emission intensity may also be explained by analyzing the excitation spectra caused by the broadening in the absorption bands followed by the overlapping between the defect states produced by the codopants with the rare earth ions charge transfer states[29], which is beyond the scope of the present study.

The UC emission peak positions remain unaltered with the codoping of $Zn^{2+}$/$Mg^{2+}$ ions. The non occurrence of the spectral shift and presence of sharp UC emission peak are due to the effect of shielding of 4f electrons by the outer 5s and 5p orbitals. The UC intensity for all the bands is quenched beyond the optimum value of $Zn^{2+}$ and $Mg^{2+}$ ions concentration. The reduction in the UC intensity is most probably due to the imperfect atomic arrangement in the

$La_2O_3$ phosphor. As the defects present in the solid host material may lead to the quenching in the emission intensity.

The ionic radii of $La^{3+}$, $Tm^{3+}$, $Yb^{3+}$, $Zn^{2+}$ and $Mg^{2+}$ are 103 pm, 88 pm, 86.8 pm, 74 pm and 72 pm respectively. Since the ionic radii of $Tm^{3+}$, $Yb^{3+}$, $Zn^{2+}$ and $Mg^{2+}$ are smaller than the $La^{3+}$ (which has largest ionic radii compared to other rare earth ions). Also, there is valency mismatch between the $Zn^{2+}$/$Mg^{2+}$ with $La^{3+}$ ion. Therefore, the excess codoping of $Zn^{2+}$/$Mg^{2+}$ ions can introduce distortion and hence defects into the $La_2O_3$ host. Thus, when the codoping concentration of $Zn^{2+}$/$Mg^{2+}$ ions is beyond the optimum value, the UC emission intensity is reduced.

Although many researchers have demonstrated the luminescence intensity enhancement caused by $Mg^{2+}$ incorporation but no one has reported such a large enhancement with $Mg^{2+}$ codoping to the best of our literature survey[24, 29, 30]. The enhancement of about 10 times in the red UC band by co-doping of $Mg^{2+}$ ions in $CaAl_{12}O_{19}$:$Er^{3+}$:$Yb^{3+}$ phosphor has been observed by Singh et al.[24]. The photoluminescence enhancement by a factor of 1.7 and 1.3 times for the red emission band in $Eu^{3+}$ doped $Y_2O_3$ phosphor due to codoping with $Mg^{2+}$ and $Al^{3+}$ ions has been observed by Chong et al.[29]. Pan et al. have reported more than 3 times enhancement in luminescence efficiency of $CaAl_{12}O_{19}$: $Mn^{4+}$ phosphor due to the codoping of $Mg^{2+}$ ions [30]. From the FTIR spectrum (Fig 3), it is clear that the presence of -OH impurity around ~ 3613 $cm^{-1}$ which acts as a quencher has been reduced for $La_2O_3$: $Tm^{3+}$- $Yb^{3+}$- $Zn^{2+}$ -$Mg^{2+}$ phosphor compared to other samples. This also supports why the UC emission intensity has been significantly enhanced in the $La_2O_3$: $Tm^{3+}$- $Yb^{3+}$- $Zn^{2+}$ -$Mg^{2+}$ phosphor. Therefore, such a large enhancement in UC luminescence intensity, as observed in $La_2O_3$: $Tm^{3+}$- $Yb^{3+}$-$Zn^{2+}$-$Mg^{2+}$, has made the present material a promising candidate for making a good blue upconverter.

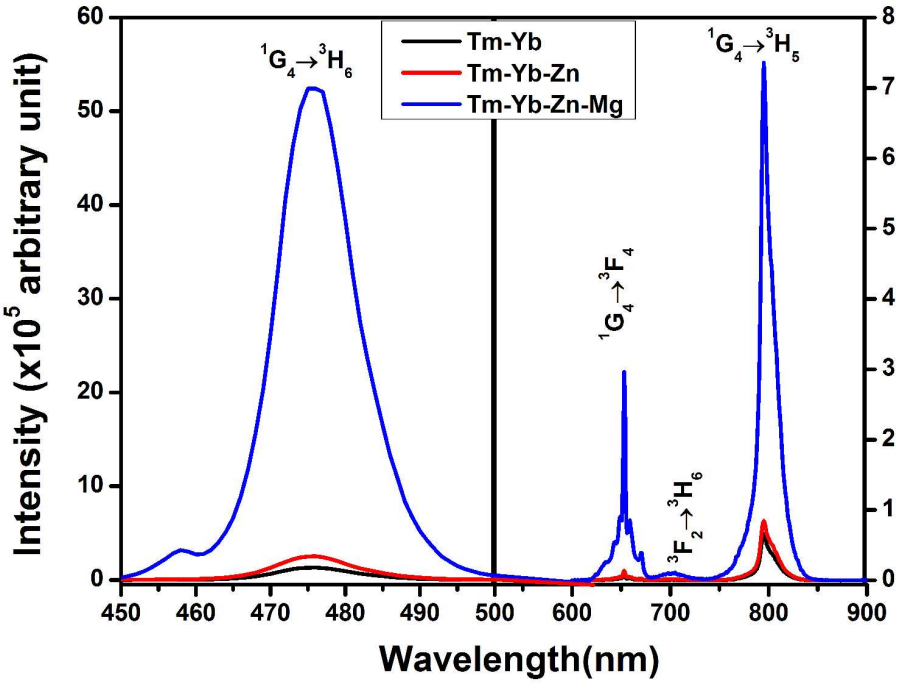


**Fig. 7:** The upconversion emission spectra of $Tm^{3+}$-$Yb^{3+}$, $Tm^{3+}$-$Yb^{3+}$-$Zn^{2+}$ and $Tm^{3+}$-$Yb^{3+}$-$Zn^{2+}$-$Mg^{2+}$ codoped $La_2O_3$ phosphors.

The decay curves analysis corresponding to the $^1G_4 \rightarrow {}^3H_6$ ( 476nm) blue transition of $Tm^{3+}$ ions in the $La_2O_3$: $Tm^{3+}$- $Yb^{3+}$, $La_2O_3$: $Tm^{3+}$- $Yb^{3+}$- $Zn^{2+}$ and $La_2O_3$: $Tm^{3+}$- $Yb^{3+}$- $Zn^{2+}$ -$Mg^{2+}$ phosphors powder samples have been made (Fig. 8). The calculated values of decay time for the blue emission from the decay curves are found to be ~ 1.78 ± 0.47 ms, ~ 1.13 ± 0.12 ms, and ~ 0.98 ± 0.06 ms for the $La_2O_3$: $Tm^{3+}$- $Yb^{3+}$, $La_2O_3$: $Tm^{3+}$- $Yb^{3+}$- $Zn^{2+}$ and $La_2O_3$: $Tm^{3+}$- $Yb^{3+}$- $Zn^{2+}$ -$Mg^{2+}$ phosphors respectively . This observed variation in decay times of

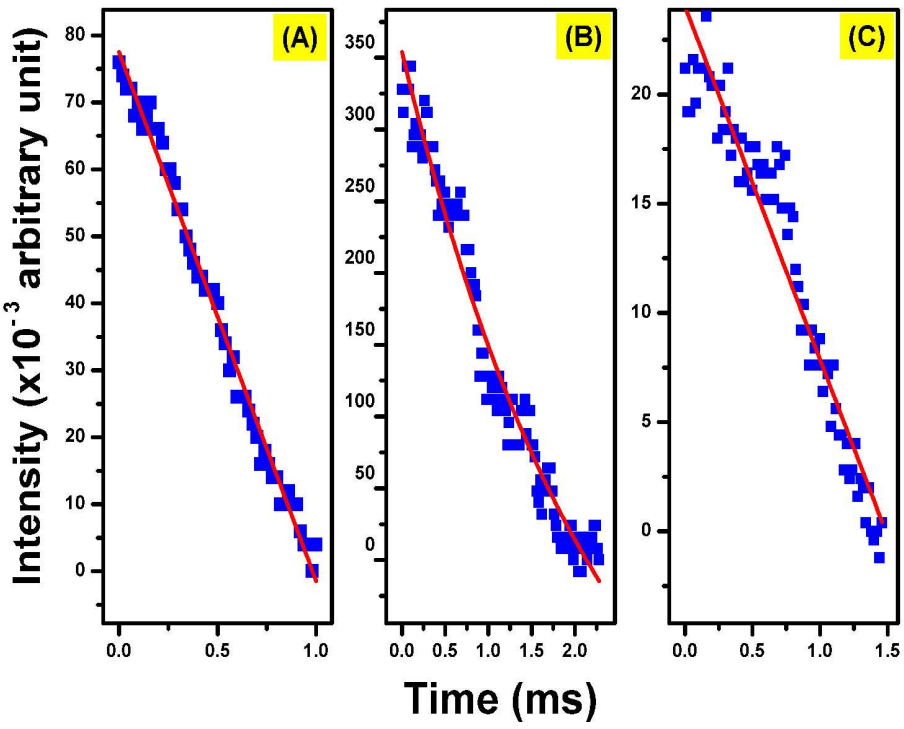


**Fig. 8:** The fluorescence decay curves corresponding to the $^1G_4 \rightarrow {}^3H_6$ ( 476nm) blue transition of thulium ion in (A)$Tm^{3+}$- $Yb^{3+}$, (B)$Tm^{3+}$- $Yb^{3+}$- $Zn^{2+}$ and (C)$Tm^{3+}$- $Yb^{3+}$- $Zn^{2+}$ - $Mg^{2+}$ codoped $La_2O_3$ phosphors.

emitting level also support the increase in radiative transition probability of emitting state due to the incorporation of $Zn^{2+}$ and $Mg^{2+}$ ions in the $La_2O_3$: $Tm^{3+}$- $Yb^{3+}$ phosphor. The decrease in decay time results in an increase of the radiative transition probability of emitting state. The reason behind this increased radiative transition probability due to $Zn^{2+}$ and $Mg^{2+}$ ions codoping is the sensitizing effect caused by the creation of oxygen vacancies as discussed in the previous part.

To compare the colour emitted by the $Tm^{3+}$-$Yb^{3+}$, $Tm^{3+}$-$Yb^{3+}$-$Zn^{2+}$ and $Tm^{3+}$-$Yb^{3+}$-$Zn^{2+}$-$Mg^{2+}$ codoped phosphors the CIE colour coordinate corresponding to these three samples at 10.04 W/cm$^2$ power density have been calculated and represented in Fig. 9 (a) from which it is clearly visible that all these three phosphors are emitting blue colour but with the

incorporation of $Zn^{2+}$ and $Mg^{2+}$ the colour is tuned towards more bluish region. This indicates that the purity of the colour emitted by the sample is improved due to the codoping with $Zn^{2+}$ and $Mg^{2+}$ ions. In order to check the tunability of the colour emitted from the $Tm^{3+}$-$Yb^{3+}$-$Zn^{2+}$-$Mg^{2+}$ codoped $La_2O_3$ phosphor the CIE colour coordinates of the sample have been calculated at different excitation power densities as shown in Fig.9 (b) which shows that the present material is an efficient blue emitter. Based on the observed results we can say that the present phosphor can be used as an efficient NIR to blue upconverter. It is observed from Fig. 9 (b) that the blue colour emitted by the sample is independent of the pump power density, so it can be used for the fabrication display devices. Also, the intense blue light emitted from the $Tm^{3+}$-$Yb^{3+}$-$Zn^{2+}$-$Mg^{2+}$ codoped $La_2O_3$ phosphor may be used in the photodynamic therapy (PDT) for diagnosis and localization of the cancer cells[7].

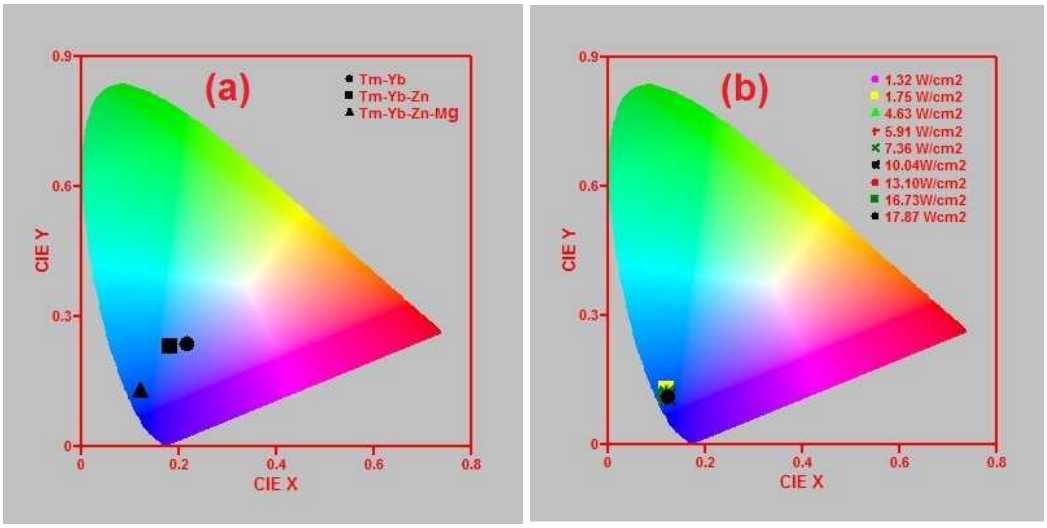


**Fig. 9: (a)** Comparison of CIE colour coordinates corresponding to $Tm^{3+}$-$Yb^{3+}$, $Tm^{3+}$-$Yb^{3+}$-$Zn^{2+}$ and $Tm^{3+}$-$Yb^{3+}$-$Zn^{2+}$-$Mg^{2+}$ codoped $La_2O_3$ phosphor , **(b)** CIE color coordinates of $Tm^{3+}$-$Yb^{3+}$-$Zn^{2+}$-$Mg^{2+}$ codoped $La_2O_3$ phosphors at different pump power densities.

For examining the quality of white light, we have calculated the Colour Correlated Temperature (CCT) values for different excitation powers densities using McCany empirical formula[31] expressed as,

$$CCT = -449\, n^3 + 3525\, n^2 - 6823\, n + 5520.33 \quad \text{..... (7)}$$

where $n = [(x-x_e) / (y-y_e)]$ is the inverse slope line with $x_e = 0.332$ and $y_e = 0.186$.

The calculated values of CCT corresponding to different colour coordinates is presented in table 1. The colour correlated temperatures for different power densities fall in the region of ~ 4171K to ~5512K. So, from the results it can be concluded that the CCT values lies in the cold white light region.

**Table 1:** The calculated CCT values for different excitation power densities.

| **Power densities (in W/ cm$^2$)** | **CIE ( x, y) coordinates** | | **CCT value( in Kelvin)** |
|---|---|---|---|
| | **x coordinate** | **y coordinate** | |
| 1.32 | 0.12 | 0.13 | 5848.70 |
| 1.75 | 0.12 | 0.13 | 5848.70 |
| 4.63 | 0.12 | 0.12 | 5093.34 |
| 5.91 | 0.12 | 0.12 | 5093.34 |
| 7.36 | 0.12 | 0.12 | 5093.34 |
| 10.04 | 0.12 | 0.11 | 4170.64 |
| 13.10 | 0.12 | 0.11 | 4170.64 |
| 16.73 | 0.12 | 0.11 | 4170.64 |
| 17.87 | 0.12 | 0.11 | 4170.64 |

## 4. Conclusion

The $Tm^{3+}$-$Yb^{3+}$, $Tm^{3+}$-$Yb^{3+}$-$Zn^{2+}$ and $Tm^{3+}$-$Yb^{3+}$-$Zn^{2+}$-$Mg^{2+}$ codoped $La_2O_3$ phosphors have been prepared successfully by combustion method. The XRD patterns of the synthesized materials shows that these phosphor powders exhibit the hexagonal phase. The crystallite sizes of the materials calculated by Scherrer's formula as well as by Williamson-Hall analysis shows that the phosphor materials are of nanocrystalline structured. The SEM analyses of the prepared materials represent the agglomerations within the materials with particle size in the micrometer range. The SEM analysis shows the increase in the particle size due to introduction of $Zn^{2+}$/$Mg^{2+}$ ions in the codoped phosphor. The impurity contents present in the prepared materials have been confirmed by the FTIR analysis. The analysis of the upconversion spectra and the decay curve collectively reveals that the maximum enhancement of the blue UC band has been observed for the $Tm^{3+}$-$Yb^{3+}$-$Zn^{2+}$-$Mg^{2+}$ codoped $La_2O_3$ phosphor upon excitation with a 980 nm NIR laser source. The CIE colour coordinates corresponding to the $Tm^{3+}$-$Yb^{3+}$-$Zn^{2+}$-$Mg^{2+}$ codoped $La_2O_3$ phosphor does not show any significant change with varying the pump power density. As a result, the present phosphor can be used in making blue light upconverter, display devices and diagnosis along with the localization of cancer cells in the photodynamic therapy.

## Acknowledgement

Authors are thankful to the University Grants Commission (UGC), New Delhi, India and Indian School of Mines, Dhanbad, India for providing financial support.

## References

(1) Blasse, G.; Grabmaier B. C. Book: Luminescent Materials, Springer-Verlag, ISBN-13: 978-3-540-58019-5.

(2) Rai, V. K.; Pandey A.; Dey R. Photoluminescence study of $Y_2O_3$:$Er^{3+}$-$Eu^{3+}$-$Yb^{3+}$ phosphor for lighting and sensing applications. *J. Appl. Phys.* **2013**, 113, 83104(1-6).

(3) Wang, G.; Qin, W.; Wang, L.; Wei, G.; Zhu, P.; Kim, R. Intense ultraviolet upconversion luminescence from hexagonal $NaYF_4$:$Yb^{3+}$/$Tm^{3+}$ microcrystals. *Opt. Express* **2008**, 16, 11907-11914.

(4) Tissue, B. M. Synthesis and Luminescence of Lanthanide Ions in Nanoscale Insulating Hosts. *Chem. Mater.* **1998**, 10, 2837-2845.

(5) Rai, V. K. Temperature sensors and optical sensors. *Appl. Phys. B* **2007**, 88, 297-303.

(6) Singh, S. K.; Kumar, K.; Rai, S. B. Multifunctional $Er^{3+}$–$Yb^{3+}$ codoped $Gd_2O_3$ nanocrystalline phosphor synthesized through optimized combustion route. *Appl. Phys. B* **2009**, 94, 165-173.

(7) Yang, D. L.; Gong, H.; Pun, E. Y. B.; Zhao, X.; Lin, H. Rare-earth ions doped heavy metal germanium tellurite glasses for fiber lighting in minimally invasive surgery. *Opt. Express* **2010**, 18, 18997-19008.

(8) Niwdbala, R. S.; Feindt, H.; Kardos, K.; Vail, T.; Burton, J.; Bielska, B.; Li, S.; Milunic, D.; Bourdelle, P.; Vallejo, R. Detection of analytes by immunoassay using up-converting phosphor technology. *Anal. Biochem.* **2001**, 293, 22-30.

(9) Binnemans, K. Lanthanide-Based Luminescent Hybrid Materials. *Chem. Rev.* **2009**, 109, 4283-4374.

(10) Zhao, C.; Zhang, Q.; Yang, G.; Jiang**,** Z. Laser-diode-excited Blue Upconversion in $Tm^{3+}$/$Yb^{3+}$-codoped $TeO_2$-$Ga_2O_3$-$R_2O$ (R=Li, Na, K) Glasses. *J. Fluoresc.* **2008**, 18, 87-91.

(11) Lin, H. J.; Chang, Y. S. Blue-Emitting Phosphor of $YInGe_2O_7$ Doped with $Tm^{3+}$ Ions. *Electrochem. Solid-State Lett.* **2007**, 10, J79-J82.

(12) Guo, H.; Dong, N.; Yin, M.; Zhang, W.; Lou, L.; Xia, S. Visible Upconversion in Rare Earth Ion-Doped $Gd_2O_3$ Nanocrystals. *J. Phys. Chem. B* **2004**, 108, 19205-19209.

(13) Silver, J.; Martinez-Rubio, M. I.; Ireland, T. G.; Fern, G. R.; Withnal, R. Yttrium Oxide Upconverting Phosphors. Part 4: Upconversion Luminescent Emission from Thulium-Doped Yttrium Oxide under 632.8-nm Light Excitation. *J. Phys. Chem. B* **2003**, 107, 1548-1553.

(14) Zhang, H.; Fu, X.; Niu, S.; Sun, G.; Xin, Q. Photoluminescence of nanocrystalline $YVO_4$:$Tm_xDy_{1-x}$ prepared by a modified Pechini method. *Mater. Lett.* **2007**, 61, 308-311.

(15) Etchart, I.; Hernandez, I.; Huignard, A.; Berard, M.; Laroche, M.; Gillin, W. P.; Curry, R. J.; Cheetham, A. K. Oxide phosphors for light upconversion; $Yb^{3+}$ and $Tm^{3+}$ co-doped $Y_2BaZnO_5$. *J. Appl. Phys.* **2011**, 109, 63104(1-7).

(16) Patra, A.; Saha, S.; Alencar, M. A. R. C.; Rakov, N.; Maciel, G. S. Blue upconversion emission of $Tm^{3+}$–$Yb^{3+}$ in $ZrO_2$ nanocrystals: Role of $Yb^{3+}$ ions. *Chem. Phys. Lett.* **2005**, 407, 477-481.

(17) Petit, V.; Doualan, J. L.; Camy, P.; Menard , V.; Moncorge, R. CW and tunable laser operation of $Yb^{3+}$ doped $CaF_2$. *Appl. Phys. B* **2004,** 78, 681-684.

(18) Simpson, D. A.; Gibbs, W. E. K.; Collins, S. F.; Blanc, W.; Dussardier, B.; Monnom, G.; Peterka, P.; Baxter, G. W. Visible and near infra-red up-conversion in $Tm^{3+}$/$Yb^{3+}$ co doped silica fibers under 980 nm excitation Opt. Express **2008**, 16, 13781-13799.

(19) Riuttamäki (née Rantanen), T. (2011), Upconverting Phosphor Technology: Exceptional Photoluminescent Properties Light Up Homogeneous Bioanalytical Assays (Doctoral Thesis), ISBN: 978-951-29-4742-3.

(20) Singh, S. K.; Singh, A. K.; Kumar, D.; Prakash, O.; Rai, S. B. Efficient UV–visible up-conversion emission in $Er^{3+}/Yb^{3+}$ co-doped $La_2O_3$ nano-crystalline phosphor. *Appl. Phys. B* **2010**, 98, 173-179.

(21) Zhang, X.; Yang, P.; Wang, D.; Xu, J.; Li, C.; Gai, S.; Lin, J. $La(OH)_3:Ln^{3+}$ and $La_2O_3:Ln^{3+}$ (Ln = Yb/Er, Yb/Tm, Yb/Ho) Microrods: Synthesis and Up-conversion Luminescence Properties. *Crys. Growth Des.* **2012**, 12, 306-312.

(22) Dey, R.; Rai, V. K.; Pandey, A. Green upconversion emission in $Nd^{3+}$–$Yb^{3+}$–$Zn^{2+}$:$Y_2O_3$ phosphor. *Spectrochim. Acta. A* **2012**, 99, 288-291.

(23) Anoop, G.; Krishna, K. M.; Jayaraj, M. K. The Effect of Mg Incorporation on Structural and Optical Properties of $Zn_2GeO_4$:Mn Phosphor. *J. Electrochem. Soc.* **2008**, 155, J7-J10.

(24) Singh, V.; Rai, V. K.; Lee, I. J.; Ledoux-Rak, I.; Al-Shamery, K.; Nordmann, J.; Haase, M. Infrared, visible and upconversion emission of $CaAl_{12}O_{19}$ powders doped with $Er^{3+}$, $Yb^{3+}$ and $Mg^{2+}$ ions. *Appl. Phys. B* **2012**, 106, 223-228.

(25) Venkateswarlu, K.; Bose, A. C.; Rameshbabu, N. X-ray peak broadening studies of nanocrystalline hydroxyapatite by Williamson–Hall analysis. *Physica B* **2010**, 405, 4256-4261.

(26) Pollnau, M; Gamelin, D. R.; Luthi S. R.; Gudel, H.U.; Hehlen, M. P. Power dependence of upconversion luminescence in lanthanide and transition-metal-ion systems *Phys. Rev B* **2000**, 61, 3337-3346.

(27) Zheng, K.; Wang, L.; Zhang, D.; Zhao, D.; Qin, W. Power switched multiphoton upconversion emissions of $Er^{3+}$ in $Yb^{3+}/Er^{3+}$ codoped β-$NaYF_4$ microcrystals induced by 980 nm excitation. *Opt. Express* **2010**, 18, 2934-2939.

(28) Yang, H. K.; Shim, K. S.; Moon, B. K.; Choi, B. C.; Jeong, J. H.; Yi, S. S.; Kim, J. H. Luminescence characteristic of $YVO_4:Eu^{3+}$ thin film phosphors by Li doping. *Thin Solid Films* **2008**, 516, 5577-5581.

(29) Chong, M. K.; Pita, K.; Kam¸ C. H. Photoluminescence of sol–gel-derived $Y_2O_3:Eu^{3+}$ thin-film phosphors with $Mg^{2+}$ and $Al^{3+}$ co-doping. *Appl. Phys. A* **2004**, 79, 433-437.

(30) Pan, Y. X.; Liu, G. K. Enhancement of phosphor efficiency via composition modification *Opt. Lett.* **2008**, 33, 1816-1818.

(31) Parchur, A. K.; Prasad, A. I.; Rai, S. B.; Ningthoujam, R. S. Improvement of blue, white and NIR emissions in $YPO_4:Dy^{3+}$ nanoparticles on co-doping of $Li^+$ ions. *Dalton Trans.* **2012**, 41, 13810-13814.